# *In vivo* video rate multiphoton microscopy imaging of human skin

**Anthony M. D. Lee,[1,2,†] Hequn Wang,[1,†] Yingqiu Yu,[1,3] Shuo Tang,[3] Jianhua Zhao,[1,4] Harvey Lui,[1,4] David I. McLean,[4] and Haishan Zeng[1,2,4,*]**

[1]*Integrative Oncology Department-Imaging Unit, British Columbia Cancer Agency Research Centre, Vancouver, British Columbia V5Z 1L3, Canada*

[2]*Department of Physics and Astronomy, University of British Columbia, Vancouver, British Columbia V6T 1Z1,Canada*

[3]*Department of Electrical and Computer Engineering, University of British Columbia, Vancouver, British Columbia V6T 1Z4, Canada*

[4]*Department of Dermatology and Skin Science, University of British Columbia and Vancouver Coastal Health Research Institute, Vancouver, British Columbia V5Z 3P1, Canada*

**Corresponding author: hzeng@bccrc.ca*

Received May 5, 2011; revised June 10, 2011; accepted June 23, 2011; posted June 27, 2011 (Doc. ID 146233); published July 25, 2011

We present a multiphoton microscopy instrument specially designed for *in vivo* dermatological use that is capable of imaging human skin at 27 frames per second with 256 pixels × 256 pixels resolution without the use of exogenous contrast agents. Imaging at fast frame rates is critical to reducing image blurring due to patient motion and to providing practically short clinical measurement times. Second harmonic generation and two-photon fluorescence images and videos acquired at optimized wavelengths are presented showing cellular and tissue structures from the skin surface down to the reticular dermis. © 2011 Optical Society of America

*OCIS codes:* 170.3880, 190.4180, 180.4315.

Since the first *in vivo* human skin images using multiphoton microscopy (MPM) were reported [1], there has been continuous growth in development and application of MPM for dermatologic uses [2,3]. The inherent optical sectioning capabilities of multiphoton excitation and the deeper penetration of the infrared wavelengths are clear advantages for bulk tissue imaging [4]. Two-photon fluorescence (TPF) from endogenous fluorophores, e.g., keratin, nicotinamide adenine dinucleotide phosphate [NAD(P)H], melanin, and elastin; and second harmonic generation (SHG) from collagen have allowed imaging of skin cells and structures in the epidermis and dermis with detail approaching that of conventional histology. For dermatologic application, the noninvasive advantage of MPM is particularly useful because standard microscopic examination necessitates an invasive biopsy procedure that in turn results in scarring and cosmetic disfigurement.

The exploration of MPM as an *in vivo* clinical skin diagnostic tool is expanding, with commercial *in vivo* MPM instruments presently being available (DermaInspect and MPTflex, JenLab GmbH, Jena, Germany) in addition to several other reported systems [1,5–7]. To date, *in vivo* studies have explored MPM for diagnosing melanoma [8], evaluating skin aging [9], and observing the diffusion kinetics of functionalized nanoparticles through the skin [10].

One significant limitation to the clinical application of existing MPM technologies is the time required to capture an image frame. Imaging speed is important for two reasons, namely, to decrease blurring effects due to subject movement and to image large or multiple skin lesions in a practical time frame. Current *in vivo* MPM instruments have varying imaging rates from 0.04–2 frames per second (fps) (0.5–24 s/frame) [1,5–7,11]. The frame rate is limited by the speed of the scanning mechanism, the strength of the multiphoton signals generated, and the upper limit of the excitation power levels acceptable for *in vivo* imaging. The aforementioned MPM systems primarily use galvanometer scanning mechanisms. For faster frame rates, rapid scanning mechanisms such as resonance scanners [12] and spinning polygon scanners [13] have been used for *ex vivo* MPM imaging, but none have been employed for *in vivo* exogenous contrast-agent-free human imaging. In this Letter, we present a resonance-scanner-based *in vivo* MPM instrument capable of video frame rates up to 27 fps at 256 pixels × 256 pixels resolution and providing good image quality. This imaging speed represents a significant improvement over currently described *in vivo* human skin imaging MPM systems for facilitating practical clinical applications.

Our multiphoton microscope setup is shown schematically in Fig. 1. The output from a tunable (720–950 nm) 80 MHz femtosecond Ti:sapphire laser (Chameleon, Coherent Inc., Santa Clara, California) was expanded with

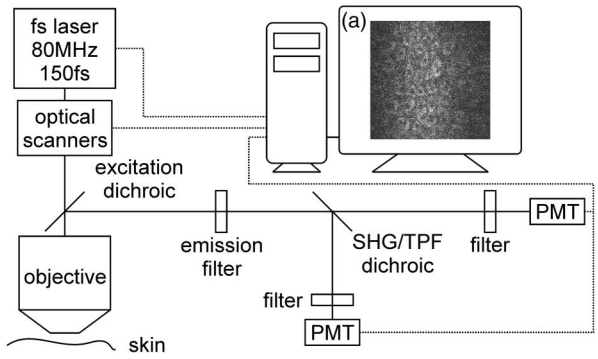


Fig. 1. *In vivo* video rate MPM setup. The SHG/TPF dichroic and filters preceding PMTs were changed or removed according to the imaging modalities. (a) Example integrated SHG/TPF image extracted from a video (27 fps) of the dorsal forearm of a 24-year-old Asian female (Media 1). Excitation wavelength = 730 nm. Both TPF and SHG photons were directed onto a single PMT. FOV = 200 $\mu$m × 200 $\mu$m. Resolution = 256 pixels × 256 pixels. Frame scan rate = 27 fps. Frame capture/display rate = 24 fps.

 

a telescope to match the optical aperture of the optical scanners. An 8 kHz resonance scanner and a galvanometer scanner were mounted as close as possible together to raster scan the laser beam (CRS8 and VM500+, Cambridge Technology, Lexington, Massachusetts). Acquiring images with 256 and 512 lines could generate a maximum frame rate of $(7916/256 =)31$ fps and $(7916/512 =)16$ fps, respectively. In our practice, the galvanometer flyback time reduced the frame rates to approximately 27 fps and 15 fps, respectively. Beyond the optical scanners, a scan and tube lens combination was used to further expand the beam to fill the rear aperture of a 60× (NA = 1.0) long working distance (~2 mm) water immersion objective (LUMPLFLN60X/W, Olympus Canada, Markham, Ontario). Adjusting the scanning angles of the resonance and galvanometer scanners (up to 15° optical) permitted a variable field of view (FOV) up to 300 $\mu$m × 300 $\mu$m. A 665 nm excitation long pass dichroic was used immediately behind the objective to reflect the epi-directed multiphoton signals towards the detection arm. The objective and detection arms were placed on the end of a cantilevered arm extending out from the optical table to allow accessibility to various skin sites.

In the detection arm, a 710 nm short pass emission filter was used to remove residual excitation light. Depending on the excitation wavelength, selected dichroic mirrors and filters were used to separate and direct the SHG and TPF signals to a pair of photomultiplier tube (PMT) modules (active area 3.7 mm × 13 mm, >15% quantum efficiency between 200 and 650 nm, H9433MOD-03, Hamamatsu Corp., Bridgewater, New Jersey). The small size of the PMT modules (19 mm × 53 mm × 51 mm) allowed for construction of a compact detection arm with close proximity of the PMTs to the objective to maximize SHG and TPF collection efficiency. Previously reported systems commonly use PMTs in photon counting or digital mode to detect the low TPF and SHG signal levels by counting single photons. As the upper count limit for a photon counting unit is typically of the order of tens of megahertz, this necessitates longer image acquisition times. We operate our PMTs in analog mode to handle the signals at the faster speed needed for video rate imaging. The SHG and TPF PMT signals were recorded by an 8 bit multichannel frame grabber (Bitflow Alta, Woburn, Massachusetts) as synchronized but separate video streams. As the resonance scanner operates bidirectionally, the forward and backward passes of each line were added during postprocessing. To further improve image quality, the acquired images were rebinned accordingly to yield a frame size of 256 pixels × 256 pixels. The images and videos presented here show some distortion near the left and right edges because they have not been corrected for the sinusoidal scan pattern of the resonance scanner. Distortion on the left side of the images is mitigated by delaying the start of the line acquisition relative to the resonance scanner turning point on the left side.

To facilitate effective optimization of excitation wavelengths for imaging different skin structures, the system was configured into a special "integrated SHG/TPF imaging modality" by removing the SHG/TPF dichroic and the filter in front of the PMT. This way, both the SHG and the TPF photons were directed onto a single PMT. At varying excitation wavelengths, the integrated SHG/TPF images can be obtained conveniently without the need to change the SHG/TPF dichroic or filters. This new imaging modality is very useful for excitation wavelength optimization in a clinical setting, where fast measurement is of essence.

For imaging, a metal ring was fixed to the skin of volunteer subjects using double-sided adhesive film. No coverslip was present between the objective and the skin surface. Water was placed within the ring prior to coupling it with a magnetic holder affixed to the instrument. The holder was mounted to a manually actuated three-dimensional translation stage to control the imaging location and depth. The laser power incident on the skin at all wavelengths was adjusted to 40 mW using a half-wave plate/polarizer combination at the laser exit. The study was approved by the University of British Columbia Research Ethics Board (#H96-70499). Informed consent was obtained from each volunteer subject.

The dorsal forearms of volunteer subjects were imaged. We found that the optimal excitation wavelengths for imaging the cellular layers in the epidermis were 730–740 nm, consistent with the excitation maxima of fluorophores within the epidermis such as keratin and NAD(P)H [11]. Dermal structures such as collagen and elastin are best imaged by 800–900 nm excitation.

The image in Fig. 1(a) was acquired in 0.036 s while those shown in Figs. 2–4 were acquired in 0.067 s. The FOV for all images presented is 200 $\mu$m × 200 $\mu$m. Figure 1(a) shows an integrated SHG/TPF image from epidermis under 730 nm excitation. TPF images of epidermis using 740 nm excitation are shown in Fig. 2. Images near the skin surface [Figs. 2(a)–2(c)] show a somewhat structureless stratum corneum (SC) overlaying the larger cells of the stratum granulosum (SG) and stratum spinosum (SS), while smaller cells of the stratum basale (SB) are present at the epidermal/dermal

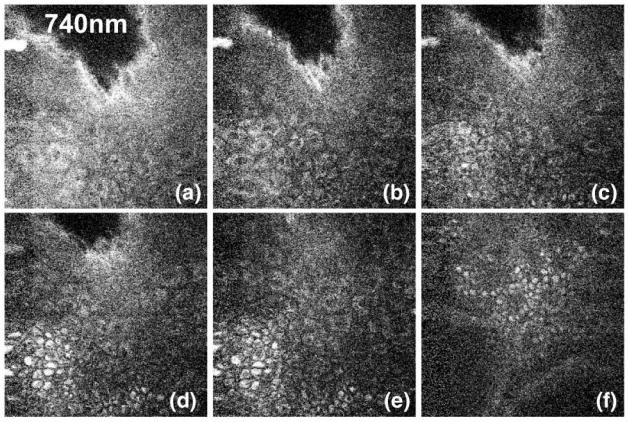


Fig. 2. TPF images from epidermis (oblique orientation) extracted from an *in vivo* video from the dorsal forearm of a 25-year-old Asian female increasing in depth from (a) near the surface to (f) near the dermal/epidermal boundary (Media 2). A 405 nm dichroic mirror ensured only TPF signals reached the PMT. Excitation wavelength = 740 nm. FOV = 200 $\mu$m × 200 $\mu$m. Resolution = 256 pixels × 256 pixels. Frame scan rate = 15 fps. Frame capture/display rate = 12 fps. At this wavelength, the cells of the epidermis are well visualized from the SC down to the SB.

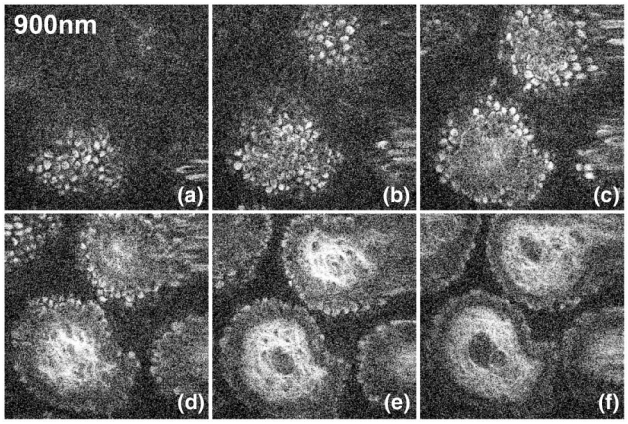


Fig. 3. Integrated SHG/TPF images of the epidermal ridges and the papillary dermis extracted from an *in vivo* video of the dorsal forearm of a 28-year-old Asian male (Media 3). The imaging depth increases from (a) to (f) starting from the dermal/epidermal boundary. Excitation wavelength = 900 nm. TPF and SHG photons were directed onto a single PMT. FOV = 200 $\mu$m × 200 $\mu$m. Resolution = 256 pixels × 256 pixels. Frame scan rate = 15 fps. Frame capture/display rate = 12 fps. At this wavelength, the cells of the SB and collagen and elastin fibers are observed.

boundary [Figs. 2(d)–2(f)]. In the SG and SS, the cell nuclei are dark while the cytoplasm is fluorescent. The SB cells appear relatively bright, presumably due to melanin fluorescence. Figure 3 shows integrated TPF/SHG images under 900 nm excitation. The papillary structure at the epidermal/dermal boundary is clearly visible. Although cells in the upper epidermis are not visualized at this wavelength, the basal cells are clearly seen, as are the fibrous structures in the dermis. False color overlay images of TPF and SHG acquired using 880 nm excitation are shown in Fig. 4. The images collected from the reticular dermis show elastin fibers in the TPF channel and collagen fiber bundles in the SHG channel.

Excerpts from the postprocessed videos from which Figs. 1(a) and 2–4 were generated are shown in Media 1, 2, 3, and 4, respectively. The frames of Media 1 were captured with 256 lines, yielding a scan frame rate of 27 fps (frame acquisition time = 0.036 s). Latency in the frame grabber we used resulted in dropped frames that reduced the captured frame rate to 24 fps. Utilizing a different frame grabber should readily capture the full frame rate. Media 2, 3, and 4 were captured with 512 lines, yielding a frame scan rate of 15 fps (frame acquisition time = 0.067 s, captured frame rate = 12 fps). The image quality improvement when scanning at the slower frame rate is noticeable as expected with double the acquisition time per frame. Clearly evident in all of the videos are the frame-to-frame jumps in the $z$ imaging plane due to subject motion, thus emphasizing the need for fast imaging frame rates. Even when subject motion is consciously reduced, cardiac pulsations can be seen in some instances. Imaging at a slower frame rate could result in significant blurring of the image. In summary, we believe that the high frame rate imaging capabilities provided by our optimized *in vivo* MPM instrument and the new integrated SHG/TPF imaging modality are unique amongst currently available

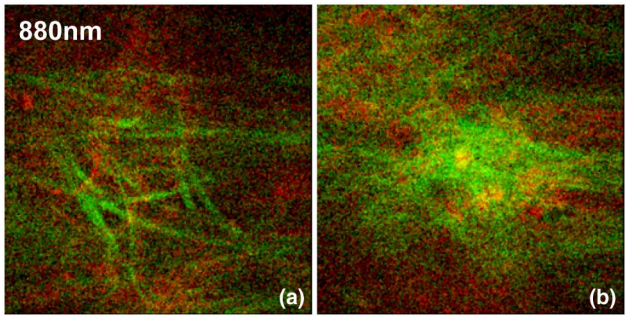


Fig. 4. False color overlay of SHG (green) and TPF (red) images from the reticular dermis extracted from an *in vivo* video of the dorsal forearm of a 63-year-old Caucasian male (Media 4). A 458 nm dichroic mirror was used to separate the SHG and TPF signals. 440/40 nm bandpass and 458 nm long pass filters were placed in front of the SHG and TPF PMTs, respectively. Excitation wavelength = 880 nm. FOV = 200 $\mu$m × 200 $\mu$m. Resolution = 256 pixels × 256 pixels. Frame scan rate = 15 fps. Frame capture/display rate = 12 fps. Collagen (SHG) and elastin (TPF) fibers are clearly seen.

systems and are necessary embodiments to the practical use of MPM in a clinical setting.

This work was funded by the Canadian Dermatology Foundation, the VGH & UBC Hospital Foundation, the BC Hydro Employees Community Services Fund, and the BC Cancer Agency. A. M. D. Lee acknowledges the Michael Smith Foundation for Health Research (MSFHR) and the CIHR Skin Research Training Centre for postdoctoral funding. H. Wang acknowledges CIHR Skin Research Training Centre for doctoral funding.

†These authors contributed equally to this work.

## References

1. B. R. Masters, P. T. So, and E. Gratton, Biophys. J. **72**, 2405 (1997).
2. K. Konig, J. Biophotonics **1**, 13 (2008).
3. T.-H. Tsai, S.-H. Jee, C.-Y. Dong, and S.-J. Lin, J. Dermatol. Sci. **56**, 1 (2009).
4. F. Helmchen and W. Denk, Nat. Methods **2**, 932 (2005).
5. S.-Y. Chen, H.-Y. Wu, and C.-K. Sun, J. Biomed. Opt. **14**, 060505 (2009).
6. T. Yasui, Y. Takahashi, M. Ito, S. Fukushima, and T. Araki, Appl. Opt. **48**, D88 (2009).
7. A. N. Bader, A.-M. Pena, C. J. van Voskuilen, J. A. Palero, F. Leroy, A. Colonna, and H. C. Gerritsen, Biomed. Opt. Express **2**, 365 (2011).
8. E. Dimitrow, M. Ziemer, M. J. Koehler, J. Norgauer, K. Konig, P. Elsner, and M. Kaatz, J. Invest. Dermatol. **129**, 1752 (2009).
9. M. J. Koehler, S. Hahn, A. Preller, P. Elsner, M. Ziemer, A. Bauer, K. Konig, R. Buckle, J. W. Fluhr, and M. Kaatz, Exp. Dermatol. **17**, 519 (2008).
10. K. Konig, A. Ehlers, F. Stracke, and I. Riemann, Skin Pharmacol. Physiol. **19**, 78 (2006).
11. K. Konig, M. Speicher, M. J. Kohler, R. Scharenberg, and M. Kaatz, J. Biophotonics **3**, 759 (2010).
12. G. Y. Fan, H. Fujisaki, A. Miyawaki, R.-K. Tsay, R. Y. Tsien, and M. H. Ellisman, Biophys. J. **76**, 2412 (1999).
13. B. Yu, K. Hean Kim, P. T. C. So, D. Blankschtein, and R. Langer, J. Invest. Dermatol. **118**, 1085 (2002).